communications earth & environment

Article

A Nature Portfolio journal

https://doi.org/10.1038/s43247-025-02709-z

Mirror image molecules expose state of rainforest stress

Joseph Byron[1] ✉, Giovanni Pugliese[1], Carolina de A. Monteiro[1], Michelle Robin[2], Eliane Gomes Alves[2], Johanna Schuettler[1], S. Christoph Hartmann[1], Achim Edtbauer[1], Bianca E. Krumm[1], Nora Zannoni[3], Anywhere Tsokankunku[1], Cléo Q. Dias-Junior[4], Carlos A. Quesada[5], Hartwig Harder[1], Efstratios Bourtsoukidis[6], Jos Lelieveld[1,6] & Jonathan Williams[1,6] ✉

Monoterpenes are key to plant communication and defence against biotic (e.g., herbivory) and abiotic (e.g., heat, drought) stress. Chiral monoterpenes, like alpha-pinene, exist as mirror image pairs, known as enantiomers. Enantiomers have the same atmospheric reactivity, but are produced and emitted by different enzymes and internal leaf mechanisms. Abiotic stress can alter their relative emissions, suggesting enantiomer ratios could indicate stress severity. Here we present (−)- and (+)-alpha-pinene and methyl salicylate measurements from the Amazon rainforest over time-of-day, season, and the 2023-24 El Niño. Correlations between alpha-pinene enantiomers shifted with stress, aligning with weakening carbon dioxide uptake by vegetation and transition between de novo and storage emissions. Low- and high-stress zones, along with a recovery zone, were defined through alpha-pinene enantiomer correlations, revealing a metric for ecosystem stress. This chiral ratio reveals diel, seasonal, El Niño, and edge effect stresses, offering a method to gauge drought severity due to climate change.

The Amazon rainforest harbours over 50% of Earth's tropical vegetation and over 10% of Earth's terrestrial biodiversity[1,2]. It is critical to global carbon sequestration, storing up to 200 Pg of carbon[3,4]. However, recent studies suggest it has become a net carbon emitter due to drought-induced dieback, increased fire frequency, and deforestation[3]. Climate models predict more frequent and intense droughts in the region, while rising temperatures are already being observed[5–7]. Understanding how the rainforest biome uptakes and emits carbon under stress is, therefore, essential.

A key physiological process in plants is the emission of volatile organic compounds (VOCs), with tropical rainforests contributing to 80% of global VOC fluxes[8]. One important subset of VOCs is monoterpenes ($C_{10}H_{16}$), emitted by vegetation as protection against biotic and abiotic stresses[9–12]. Tropical vegetation emits monoterpenes through two known processes: direct emission using freshly assimilated carbon following photosynthesis, termed de novo emission; and emission from non-specific aqueous and lipid phase storage pools[13]. Some monoterpenes are chiral, existing in mirror image pairs, (−) and (+), known as enantiomers. The most abundant monoterpene in the ambient air of tropical rainforests is alpha-pinene, with (−)-alpha-pinene usually dominating over (+)-alpha-pinene[14–17]. Recently, experiments using isotopically labelled carbon dioxide (CO_2) within an enclosed rainforest biome revealed that (−)-alpha-pinene was partially emitted de novo, whereas (+)-alpha-pinene was solely emitted from storage pools[15].

Abiotic stress is caused by non-living factors such as non-optimal temperatures, ozone, and droughts. Central Amazonia undergoes an annual cycle of wet and dry seasons, with the latter bringing increased temperatures, elevated ozone, and reduced rainfall, leading to regular cycles of abiotic stress. The El Niño Southern Oscillation (ENSO) affects the Amazon basin by decreasing rainfall and soil moisture while increasing temperatures[18,19]. Drought, ozone, and heat stress affect VOC emissions from vegetation[15,20–23], but existing VOC-based stress metrics, such as methyl salicylate (MeSA) and green leaf volatiles, such as hexanal, are limited by their susceptibility to atmospheric oxidation and variability in emission strength from different plant species and chemotypes[21,24–28]. Thus, there is no general established method to translate such ambient VOC signals into the degree of stress suffered by vegetation. Abiotic stress can alter the composition of

[1]Atmospheric Chemistry, Max Planck Institute for Chemistry, Mainz, Germany. [2]Biogeochemical Processes Department, Max Planck Institute for Biogeochemistry, Jena, Germany. [3]National Research Council of Italy—Institute of Atmospheric Sciences and Climate, Bologna, Italy. [4]Federal Institute of Pará (IFPA), Belém, Pará, Brazil. [5]National Institute of Amazonian Research (INPA), Manaus, Brazil. [6]Climate and Atmosphere Research Center, The Cyprus Institute, Nicosia, Cyprus. ✉e-mail: j.byron@mpic.de; jonathan.williams@mpic.de

monoterpene emissions from vegetation in two ways. First, it can lead to the breakdown of storage pools, releasing an increased fraction of (+)-alpha-pinene[15]. Second, it can increase de novo emissions of specific monoterpenes, as some enzymes produce greater yields of monoterpenes at higher temperatures[20]. These increases in reactive VOC emissions can help plants endure abiotic stress by protecting against damage from reactive oxygen species, which destroy cell membranes and can ultimately lead to plant death[11,12,29]. Therefore, in contrast to single VOC stress indicators, such as MeSA and hexanal, the alpha-pinene chiral ratio offers greater utility and range since it is abundant throughout all ecosystems and more closely linked to the underlying emission mechanisms. Through comparisons of alpha-pinene enantiomer ratios, we propose a new metric to assess the degree of rainforest ecosystem stress that is uncoupled from atmospheric oxidation and variability in emission strength, as enantiomers have identical oxidation rates and alpha-pinene is ubiquitous in the rainforest atmosphere[14].

Record-breaking temperatures and historically extreme drought were experienced by the Amazon basin during 2023[18]. Over two years from January 2023 to October 2024, we sampled and quantified (-)-alpha-pinene, (+)-alpha-pinene, and MeSA abundances at 1.5-to-3-hour intervals with sorbent tubes and off-line gas chromatography time-of-flight mass spectrometry. The sampling took place at 24 m within the rainforest canopy at the Amazon Tall Tower Observatory (ATTO) site, 150 km northeast of Manaus, central Amazonia[30]. We captured different stages of the El Niño cycle, before (January 2023), near the peak drought intensity (October 2023), near the end (April–May 2024) and after (October 2024) (Fig. 1a). Furthermore, using our newly proposed metric-the (+)-alpha-pinene to (−)-alpha-pinene ratio, hereafter referred to as the alpha-pinene chiral ratio, we provide an alternative explanation for the reported surprising change in chiral ratio observed as a function of height and season at the 320 m ATTO tower in 2017 and 2018[14]. Additionally, we demonstrate how abiotic stress varies amongst different rainforest locations.

Results and discussion

Severe stress during October 2023

The 2023 El Niño dry season was markedly hotter and drier than ENSO-neutral dry seasons[18]. In October 2023, canopy temperatures peaked at 37.5 °C, 2.5 °C warmer than in October 2024, while median relative humidity dropped to 62%, 12% lower than in October 2024 (Fig. 1b, e)[27]. Extreme drought conditions were also reflected in the soil moisture levels, which fell to a median of 0.15 $m^3 m^{-3}$ in October 2023, lower than in other periods (Fig. 1d)[18]. Increased vegetation stress was apparent during ENSO-influenced October 2023, with ambient ozone concentrations reaching a median of 26.6 ppb, 16.4 ppb higher than in October 2024 (Fig. 1g), despite comparable photosynthetically active radiation (PAR) (Fig. 1c). These elevated ozone levels are likely due to increased wildfires in the region[31]. MeSA levels peaked in October 2023 compared with much lower values in other periods (Fig. 1f). The median isoprene abundances measured at 80 m on the nearby tall tower during the two wet seasons (Jan 23 and Mar 24) were comparable, although higher abundances were occasionally measured during Mar 24, aligning with the MeSA measurements (Supplementary Fig. 1). Timelines showing the daily maxima for 10 cm soil moisture, and 26 m temperature and relative humidity from January to December 2024 are given in Supplementary Fig. 2. These observations underscore severe ecosystem stress during October 2023, consistent with Amazon-wide conditions during the 2023–24 El Niño[18].

Chiral ratio varies with CO_2 uptake

During January 2023, October 2023, April–May 2024, and October 2024, atmospheric samples were collected every 1.5–3 h within the rainforest canopy at 24 m to investigate how (-)-alpha-pinene and (+)-alpha-pinene covary throughout an El Niño drought event (Fig. 2a, b, c, d). Since these enantiomers share identical oxidation rates, changes in chiral ratio reflected variations in emission mechanisms[14]. This is because the alpha-pinene

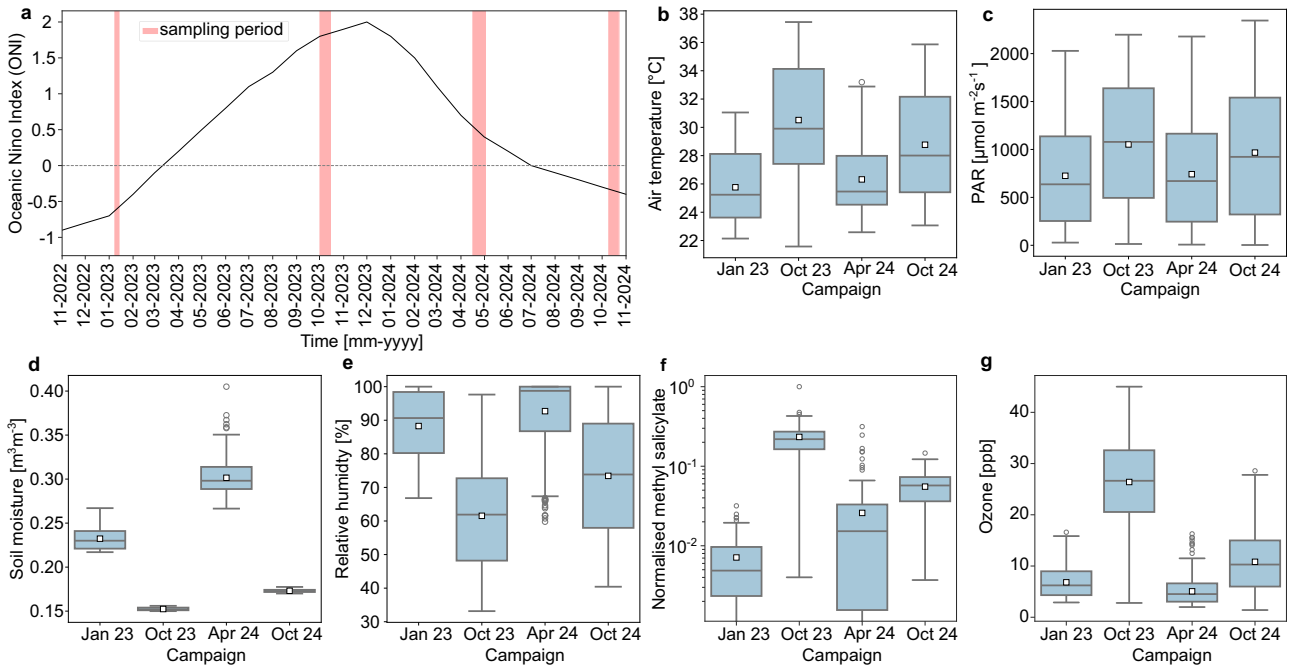

Fig. 1 | Development of El Niño–Southern Oscillation (ENSO) with its meteorological characteristics and stress-related volatile emissions. a The ENSO timeline is shown as the Oceanic Niño Index (ONI), which represents the 3-month average temperature anomaly in the oceanic surface waters. The ONI is shown with the black thick line while the sampling periods are indicated with the red shaded areas. Source: National Oceanic and Atmospheric Administration[61]. **b** Air temperature measured at 26 m within rainforest canopy. **c** Photosynthetically active radiation (PAR) measured at 81 m above the rainforest canopy. **d** Soil moisture content at 10 cm depth measured near to the 80 m walk-up measurement tower. **e** Relative humidity measured at 26 m within the rainforest canopy close to the volatile organic compound (VOC) sampling inlet. **f** Methyl salicylate (MeSA) abundance normalized to the maximum measured value across all measurement periods, at 23 m within rainforest canopy. **g** Ambient ozone mixing ratio measured at 24 m within the rainforest canopy close to the VOC sampling inlet. The box plots give the median and 25th and 75th percentiles, the squares show the mean, the whiskers show the maximum and minimum acquired data points that are not considered outliers, and the circles represent outliers.

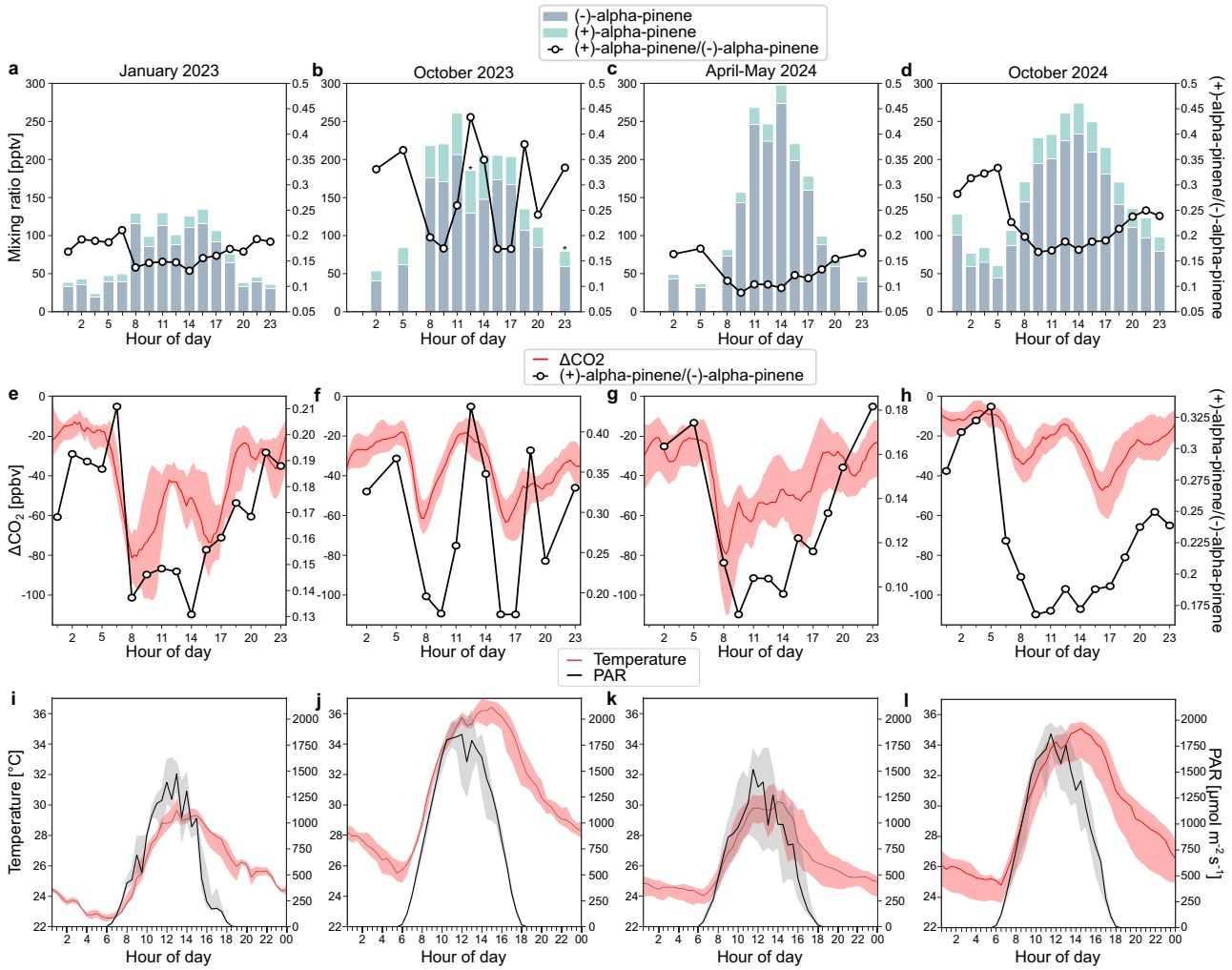

Fig. 2 | Effect of weakening CO_2 uptake on the alpha-pinene chiral ratio. Diurnal cycles for each measurement period showing median mixing ratios for (−)-alpha-pinene, (+)-alpha-pinene, and alpha-pinene chiral ratio. **a** January 2023. **b** October 2023. **c** April–May 2024. **d** October 2024. At 12:30 and 23:00, total alpha-pinene was measured with a non-chiral method and the chiral ratio was calculated from subtracting the median (+)-alpha-pinene of the adjacent time periods from the total measured alpha-pinene. These time periods are indicated by * (see "methods" for details). Diurnal cycles for each measurement period showing differences between the CO_2 mixing ratios at 24 m and 0.5 m (ΔCO_2), and the median alpha-pinene chiral ratio. The shaded region represents the 25th and 75th percentiles. **e** January 2023. **f** October 2023. **g** April–May 2024. **h** October 2024. A composite figure of the chiral ratio diurnal cycles for each period is given in Supplementary Fig. 3. Diurnal cycles of median temperature measured at 26 m and PAR measured at 81 m, shaded regions around the median lines show the 25th and 75th percentiles. **i**. January 2023. **j** October 2023. **k** April–May 2024. **l** October 2024.

enantiomers partition differently between de novo and storage pool emissions, which respond differently by abiotic stress[15]. Storage pool emissions depend on the volatilization of compounds from lipid or aqueous phase storage pools and subsequent diffusion, processes coupled to leaf temperature[32–34]. In contrast, de novo emissions are driven by PAR, the availability of freshly assimilated carbon, and the proximity of leaf temperature to the optimum temperature for the enzymes involved in their biosynthesis[32–34]. Consistent with previous studies in tropical ecosystems, (-)-alpha-pinene was the dominant enantiomer[14,15,17].

A surprisingly intense midday increase in chiral ratio occurred during the El Niño-influenced October 2023 samples, coinciding with an overall decline in (−)-alpha-pinene mixing ratios (Fig. 2b). This pattern was absent in other sampling periods (Fig. 2e–h). A similar trend was observed for ΔCO_2 (Fig. 2f), while a midday decrease was observed for average stomatal conductance (Supplementary Fig. 4), indicating that as stomatal conductance decreased over midday, CO_2 uptake and photosynthesis declined, limiting carbon availability for de novo (-)-alpha-pinene production. This decrease in (−)-alpha-pinene production resulted in the observed chiral ratio increase, as storage pool (+)-alpha-pinene emissions are unaffected by stomatal conductance and temporary declines in photosynthesis[35]. Notably, a short lag was observed between the midday increase in ΔCO_2 and the chiral ratio in both October 2023 and April–May 2024 (Fig. 2f, g). This suggests a temporal delay between stomatal closure and reduction in (-)-alpha-pinene de novo emissions. This could be caused by reduced carbon assimilation freeing up reducing power which can be directed towards the biosynthesis of monoterpenes, temporarily maintaining (-)-alpha-pinene de novo emissions, as has been seen previously for isoprene[36,37]. This pattern aligns with the behaviour of MeSA, a plant signalling compound known to induce stomatal closure[38], which peaked at 08:00 just before the chiral ratio began rising at 09:30 as stomata closed (Supplementary Figs. 4, 5). Since MeSA is relatively water-soluble[35], its midday decline is likely due to stomatal closure trapping it within the leaf's aqueous phase (Supplementary Fig. 5). The chiral ratio decreased in the afternoon, due to increased stomatal conductance and photosynthesis, and increased transpiration, when temperatures peaked. After sunset, CO_2 uptake decreased, corresponding with a temporary spike in the chiral ratio, reflecting reduced de novo (−)-alpha-pinene emissions as PAR diminished before equilibrium between (−)-alpha-pinene and (+)-alpha-pinene was restored overnight. The chiral ratio pattern observed here represents a striking alteration in the ecosystem's photosynthetic strategy, distinct from other periods.

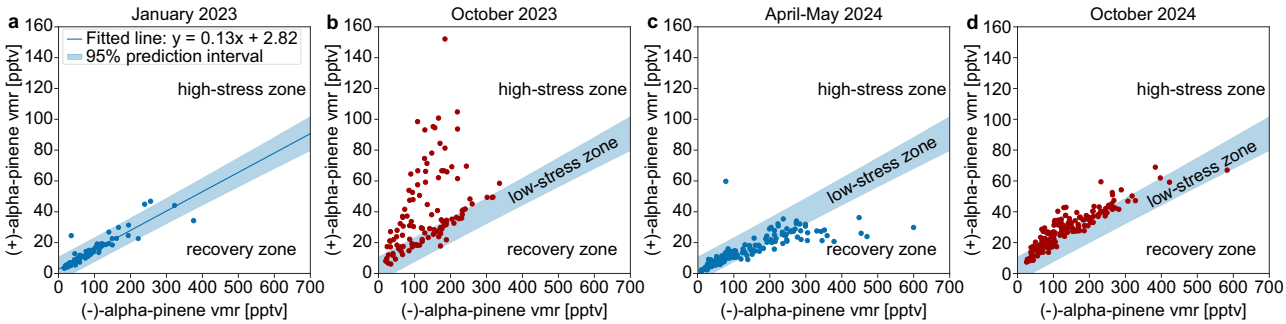

Fig. 3 | Branching of chiral ratio from low stress zone during October 2023, associated with stomatal closure and enhanced emissions from storage pools relative to de novo emissions. Correlations of (+)-alpha-pinene and (−)-alpha-pinene across sampling periods with conceptual zones labelled for high stress, low stress, and recovery. **a**. January 2023 (wet season, before El Niño). **b** October 2023 (dry season, near to peak El Niño). **c** April–May 2024 (wet season, end of El Niño). **d** October 2024 (dry season, after El Niño). The blue shaded bar indicates the low-stress zone defined using the 95% prediction band from the data in Fig. 3a.

In January 2023 and October 2024, the relative increase in ΔCO_2 over midday was weaker than in October 2023, aligning with the small midday rise in the alpha-pinene chiral ratio. This suggests that abiotic stress was less severe in January 2023 and October 2024 than in October 2023, leading to weaker midday stomatal closure of the surrounding vegetation (Fig. 2e, f, h). Total alpha-pinene mixing ratios were lower in October 2023 than in October 2024 due to higher ozone levels, and thus, OH, thereby reducing the mixing ratios of both enantiomers through increased reactions in the atmosphere (Fig. 1g).

The night-time alpha-pinene chiral ratio peaked at 05:00 during most sampling periods, except in January 2023, when it peaked at 06:30. This delay indicates that de novo emissions had a delayed start due to lower levels of photosynthetically active radiation (PAR) and temperature (Fig. 2i). Previous studies have shown that isoprene flux, a purely de novo emitted compound by plants[39], is reduced to zero during night-time hours in the Amazon rainforest due to photosynthesis becoming inactive[27,40]. Therefore, night-time peaks in the chiral ratio suggest storage pools were the dominant emission source before PAR activated the de novo synthesis and temperature increased (Fig. 2i, j, k, l). Higher night-time chiral ratios were observed in October 2023 and October 2024 compared to January 2023 and April–May 2024, indicating greater volatilisation from storage pools due to higher temperatures. As PAR rose, de novo emissions of (−)-alpha-pinene increased, causing the chiral ratio to decline into the early morning across all periods.

The highest median mixing ratios of (+)-alpha-pinene and (−)-alpha-pinene unexpectedly occurred during ENSO-influenced April–May 2024 compared to January 2023(Fig. 2a, c). This clearly reflects elevated de novo (−)-alpha-pinene emissions in April–May 2024 compared to January 2023, potentially due to post-stress adaption or new leaf growth[41]. Indeed, ozone and (+)-alpha-pinene levels remained comparable between January 2023 and April–May 2024, ruling out atmospheric oxidation as a contributing factor. Additionally, daytime chiral ratios during April–May 2024 were the lowest across the ENSO cycle, further supporting the relative increase in de novo emissions during this period. In April–May 2024, the chiral ratio again reflected the pattern observed for ΔCO_2 (Fig. 2g.), with greater CO_2 uptake, potentially due to the flushing of new leaves with greater photosynthetic capacity than older leaves during other sampling periods[41–44]. These findings highlight severe vegetation stress during October 2023 and recovery by April–May and October 2024.

Chiral ratio indicates degree of stress

Plotting the mixing ratios of (+)-alpha-pinene against (−)-alpha-pinene provides insights into shifts between storage pool emissions and de novo emissions. During January 2023, the two enantiomers were strongly correlated (Fig. 3a), contrary to previous findings[15,17]. This period of low ambient temperatures and high soil moisture (Fig. 1b, d) suggests minimal abiotic stress. The low mixing ratios and tight correlation also indicated optimal conditions for the biosphere and minimal abiotic stress; therefore, a 95% prediction band around the January 2023 data was defined as the "low stress zone".

In October 2023, the correlation weakened and shifted, with (+)-alpha-pinene increasing relative to (−)-alpha-pinene due to higher night-time storage emissions and midday weakening of CO_2 uptake due to stomatal closure (Fig. 3b). Some data points still fell within the low-stress zone, indicating variable stress resistance amongst vegetation, or periods of elevated de novo (−)-alpha-pinene emissions. A "high-stress zone" was defined above the low stress zone, reflecting increased stress intensity. Despite ongoing El Niño influence in April–May 2024, ambient temperatures decreased, while soil moisture increased, indicating reduced stress-consistent with lower MeSA and ozone (Fig. 1). As expected, most data fell within the low stress zone (Fig. 3c). However, a subset fell below this range due to increased de novo (−)-alpha-pinene emissions following earlier drought stress, leading to the definition of a "recovery zone" requiring further investigation. In October 2024, most measurements remained in the low stress zone, though a few measurements exceeded this range, suggesting moderate abiotic stress due to the characteristic warmth and dryness of the dry season (Fig. 3d). Furthermore, by plotting the chiral ratios from each sampling period against the measured 10 cm soil moisture, a threshold soil moisture value of approximately 0.2 $m^3\ m^{-3}$ was identified, below which the chiral ratios began to notably increase (Supplementary Fig. 6).

These findings demonstrate the utility of chiral ratios as indicators of ecosystem response to abiotic stress, revealing stomatal closure and elevated storage pool leakage. The angle between the gradients of high-stress data points and the low-stress zone might serve as a useful metric for stress severity. However, the low stress zone should be characterized for different vegetation, especially from different ecosystems which may have specialized storage structures such as resin ducts or trichomes.

Stress from edge effect and soil type

Measurements taken from the 320 m ATTO tower showed a greater ratio of alpha-pinene chiral ratio near the base compared to the top in October 2017, a trend not observed in March 2018[14]. This shift suggests changes in the local ecosystem. Further measurements and analysis ruled out preferential oxidation of one enantiomer over the other[14]. The authors initially attributed this to other processes, occurring locally within the 40 m fingerprinted area, such as mechanical damage stress and insect-related emissions. With a better understanding of how enantiomeric ratios respond to stress, we now propose a more specific explanation: the local atmosphere around the tower base was enriched in (+)-alpha-pinene due to greater abiotic stress on vegetation near the edge of the 20 m diameter clearing and path around the tower. These areas are more exposed to characteristic edge effects like increased radiation, wind, and drier conditions, compared to the interior forest[45–47]. This effect was more pronounced in October 2017 during the dry season, whilst in March 2018, during the wet season, stress levels were lower. Measurements in March 2018 at 80 m were mostly in the low-stress zone, with some brief periods of increased stress (Fig. 4a). In contrast,

measurements from October 2017 at 40 m largely fell within the high-stress zone. Samples taken at 80 m show a slight shift in measurements towards the low-stress zone as the influence from the local edge effect decreased, whilst samples taken from higher on the tower at 320 m were mixed between high- and low-stress zones, suggesting the interior rainforest was suffering less stress than the local vegetation on the edges, but some local convection events may have transported air enriched in (+)-alpha-pinene to 320 m. These observations suggest that the edge effect around the ATTO tower imposed greater abiotic stress on local vegetation than the conditions in October 2023 did on the more sheltered, interior, canopy vegetation.

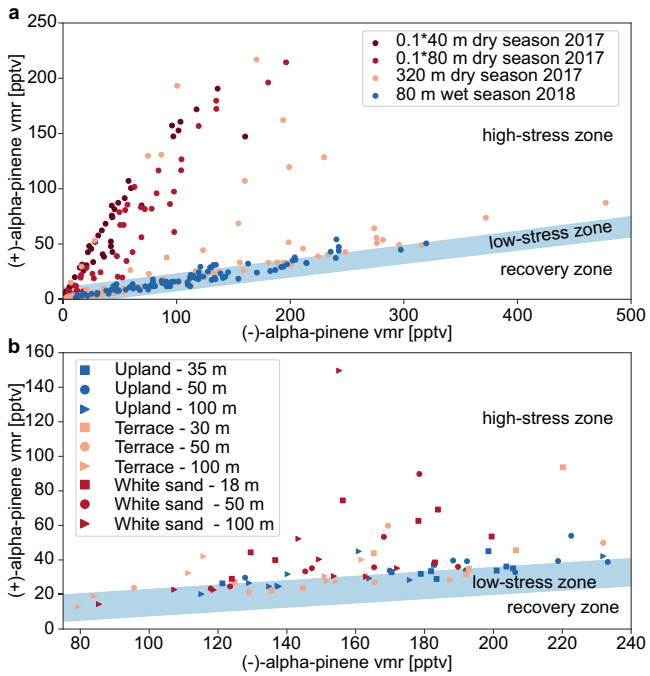

Fig. 4 | Correlations of alpha-pinene enantiomers resulting from edge effect around the 320 m ATTO tower and forest type. Correlations between (+)-alpha-pinene and (−)-alpha-pinene sampled from different locations and heights. **a** At 40, 80, and 320 m during October 2017 (dry season) and at 80 m during March 2018 (wet season). Data obtained at 40 m and 80 m from 2017 has been divided by 10 to bring it onto the same scale as the rest of the data for clarity. Source: Zannoni et al. 2020[14]. The blue shaded bar indicates the low stress zone defined using the 95% prediction band from the data in Fig. 3a. **b** Drone measurements from 3 different locations, upland forest, white-sand forest, and ancient river terrace forest, from 8th–17th October 2024 taken between 12:00–13:30 local time.

To test the chiral stress marker metric, in October 2024, drone-collected samples were obtained from three locations with differing soil and vegetation types to asses abiotic stress levels in other areas of the rainforest (Fig. 4b.). The locations included: dense, non-flooded forest upon ancient river terraces adjacent to the Uatumã river, shrubland/closed-canopy vegetation on white sands (Campina), and dense, non-flooded upland forest, near the 80 m walk-up tower at the ATTO site[22]. Upland forest samples and ancient river terrace forest samples aligned with within-canopy measurements from the 80 m walk-up tower(Fig. 3d), straddling the boundary of the low- and high-stress zones. In contrast, most white-sand forest measurements fell within the high-stress zone, as expected, due to the site's highly permeable soil with low water-holding capacity, which exacerbates vegetation stress during dry seasons[22].

These findings suggest the alpha-pinene chiral ratio is a valuable new indicator for assessing various types of ecosystem stress, including diurnal fluctuations, seasonal changes, El Niño events, edge effect dynamics, and soil-water availability. A schematic summarising the different investigated effects on the alpha-pinene chiral ratio is provided in Fig. 5. This metric provides a means to quantify plant responses to stress by serving as a proxy for the ratio of storage pool to de novo emissions, which is independent from atmospheric oxidation. Upon further development, instruments which capture the online chiral emission ratio may be deployable at measurements sites and used to monitor the stress of vegetation[48]. Remarkably, emission models do not currently incorporate stress-specific mechanisms, presenting a critical gap in their capacity to predict emissions under varying climatic conditions[8,49]. By integrating the chiral ratio as a stress-responsive factor, emission models might be refined to account for stress-induced shifts, improving their accuracy and utility for ecological and atmospheric research. This approach represents a promising step toward a more process-based BVOC emission model, which will be important for accurately forecasting atmospheric composition responses to global change.

Methods

Sampling site

The 325 m Amazon Tall Tower Observatory (ATTO) site is situated 150 km northeast of Manaus, Brazil, and 120 m above sea level within a dense *terra firme* forest[30]. The nearby 80 m walk-up tower (Instant UpRight, Dublin, Ireland) is located at S 02∘ 08′ 38.6″, W 58∘ 59′ 59.9″. The canopy surrounding the tower has a top height of approximately 35 m and 417 tree species have been identified in the surrounding area[30]. The region experiences a distinct wet season from November to May, followed by a drier period from June to October[30]. The site is characterised by typical Amazonian flora, with hyperdominant species being abundant alongside a generally diverse plant community[50]. Tropical species have been reported to emit monoterpenes (MTs) as a function of temperature[51], while also storing

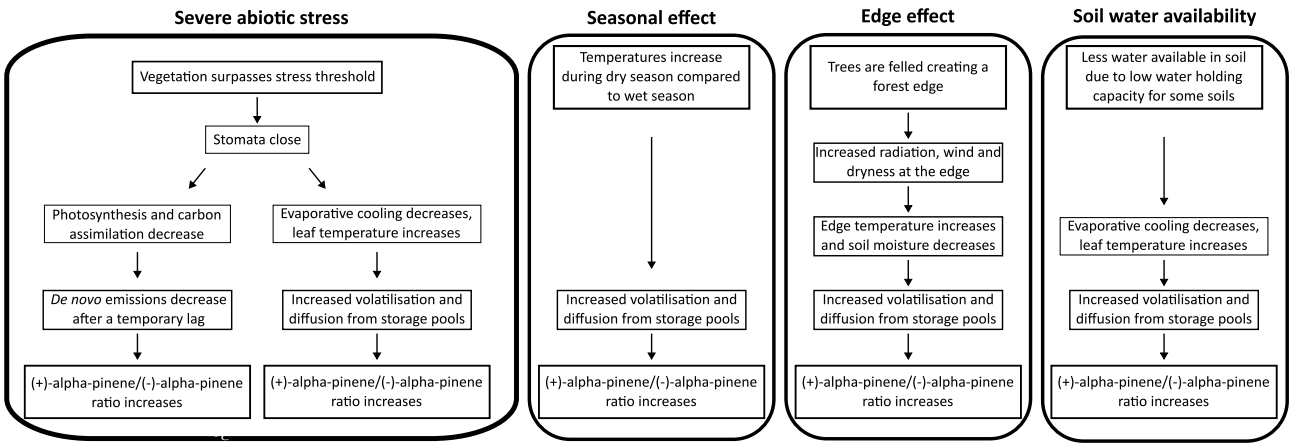

Fig. 5 | Summary of different stresses investigated: severe abiotic stress associated with the El Niño, seasonal changes, edge effect and soil water availability dependent on location.

Table 1 | Sampling overview and observed meteorological conditions

Sampling period	Season	# VOC data points	26 m temp. mean ± SD (°C)	26 m temp. range (°C)	26 m RH mean ± SD (%)	26 m RH range (%)	10 cm soil moisture mean ± SD (m^3 m^{-3})	10 cm soil moisture range (m^3 m^{-3})	81 m max.PAR mean ± SD (µmol m^{-2} s^{-1})	81 m max. PAR (µmol m^{-2} s^{-1})
January 8–13 2023	Wet	80	25.8 ± 2.4	22.1– 31.1	88.3 ± 9.9	66.8– 100	0.232 ± 0.012	0.217– 0.267	383 ± 530	2028
October 1–14 2023	Dry	112	30.5 ± 3.9	21.6 – 37.4	61.5 ± 15.4	33.2– 97.6	0.152 ± 0.002	0.150– 0.156	534 ± 697	2197
April 16–May 4 2024	Wet	158	26.3 ± 2.5	22.6 – 33.2	92.7 ± 10	59.8– 100	0.301 ± 0.018	0.266 – 0.405	376 ± 542	2179
October 9–23 2024	Dry	173	28.8 ± 3.8	23.1 – 35.9	73.4 ± 18	40.4 - 100	0.173 ± 0.002	0.170 – 0.177	480 ± 668	2345

them in internal pools[52]. A footprint analysis of the measurement tower can be found elsewhere[27].

Analysis of ambient air samples and determination of mixing ratios from walk-up tower

From January 8–13 2023, October 1–14 2023, April 16–May 4 2024, and October 9–23 2024, the ambient air from a height of 23 meters in the middle of the rainforest canopy on the 80 m walk-up tower was sampled onto sorbent cartridges using custom-built automatic samplers[14,53]. An overview of the sampling periods and meteorological conditions are given in Table 1. Samples were collected throughout a number of consecutive days every 3 h or 1.5 h, depending on sorbent tube availability. Background levels of VOCs were accounted for with sorbent tubes frequently placed into the automatic sampler through which ambient air was not actively sampled. The median peak area for each VOC in the background samples was then calculated and subtracted from the peak area of each VOC in the ambient samples. In the few cases for MeSA when the background amount was greater than the sampled amount, resulting in a negative value, the amount was set to 0. The ambient air was sampled for 30 min onto sorbent cartridges at flows ranging between 40 and 200 ml min^{-1}. Ozone scrubbers made by impregnating quartz filters with a 10% w/w sodium thiosulphate solution were used at the sampling inlets to remove ozone from the sampled air and were replaced every day[54]. The inlet line was flushed for 30 min prior to sampling to remove the dead volume. The sorbent cartridges were made from inert coated stainless steel (SilcoNert 2000 (SilcoTek™, Germany)) containing 150 mg of Tenax® TA (Buchem BV, Apeldoorn, The Netherlands) followed by 150 mg of Carbograph™ 5 TD (560 m^2/g) (L.A.R.A s.r.l, Rome, Italy) sorbent. The size of the Carbograph™ particles was in the range of 20-40 mesh. Prior to sampling, sorbent tubes were stored in an air-conditioned container at room temperature before being transported to the laboratory, stored in a freezer at −4 °C, and analysed within 3 months following the sampling date.

Sample desorption was performed using a two-stage automated thermal desorber (TD100-xr, MARKES International, U.K.), with helium 5.0 as the carrier gas. Sorbent tubes were first purged for 5 min prior to sampling for each sampling period except October 2024, when the sorbent tubes were purged for 10 min with a flow of 50 ml min^{-1} to remove any excess water. The sample was then desorbed at a temperature of 250 °C and a flow of 50 ml min^{-1} of helium for 5 min, and was pre-concentrated onto a cold trap (materials emissions, MARKES International, U.K.) at 30 °C. The cold trap was purged with carrier gas for 1 min with a flow of 50 ml min^{-1} and then rapidly heated to 250 °C. The sample was removed from the cold trap with a flow of 3.2 ml min^{-1} and injected into the column. The separation of the sampled compounds was achieved using a 60 m β-DEX™ 120 column (Sigma-Aldrich Chemie GmbH, Germany) with 0.25 mm internal diameter and a film thickness of 0.25 µm. The temperature program used was as follows: 50 °C for 5 min then 50 °C to 110 °C at 1.5 °C min^{-1} and 110 °C to 220 °C at 10 °C min^{-1}. The column flow was set to 1.2 ml min^{-1} and the desorb split flow was 2 ml min^{-1}. All sorbent tubes were desorbed in a random order within each set of cartridges from each sampling period. Samples taken at 12:30 and 23:00 during October 2023 were processed using the same thermal desorption parameters as the rest of the samples except the sorbent tube desorption temperature was set to 200 °C and the trap desorption flow was 5.2 ml min^{-1} with a split flow 4 ml min^{-1}. Peak separation for these samples was achieved using a non-chiral 60 m DB5-ms column (Agilent Technologies, UK) with 0.25 mm internal diameter and a film thickness of 0.25 µm. The column flow was set to 1.2 ml min^{-1}. The following temperature program was used: 50 °C to 150 °C at 4 °C min^{-1} and 150 °C to 200 °C at 8 °C min^{-1} and then held at the final temperature for 7 min. The column flow was 1.2 ml min^{-1}. This data was calibrated separately from the chiral data. Therefore, total alpha-pinene was measured for these samples instead of separate measurements for (−)-alpha-pinene and (+)-alpha-pinene. The median amount of (−)-alpha-pinene and (+)-alpha-pinene was calculated by taking the median (+)-alpha-pinene at 11:00 and 14:00 and subtracting it from the total alpha-pinene measured at

12:30 to obtain the median mixing ratio of (−)-alpha-pinene. The same procedure was performed for the samples at 23:00, with the median (+)-alpha-pinene from the data at 20:00 and 02:00 being taken and subtracted from the total alpha-pinene measured at 23:00. This was done to validate the chiral method and to make sure that all the enantiomers were accounted for and accurately quantified and the non-chiral data agreed with the diurnal trends of the chiral data when the enantiomers were summed together. This was also done to search for other VOCs which might be abundant at much smaller mixing ratios, such as diterpenes, which would potentially appear in even lower amounts when separated into enantiomers and maybe be below the limit of detection.

Detection was achieved using a time-of-flight mass spectrometer (Bench TOF-Select, MARKES International, U.K.). A standard gas calibration mixture (Apel-Riemer environmental Inc., USA; 2019) containing (-)-alpha-pinene and (+)-alpha-pinene was used to identify and calibrate the samples. Stepwise calibrations for (−)-alpha-pinene and (+)-alpha-pinene were performed before and after analysing of a set of samples, with single-point calibrations every ~10 samples to track retention time shifts and unexpected deviations in mass spectrometer sensitivity. The mass spectrometer sensitivity decrease was corrected by fitting a linear line between the first and last calibrations. MeSA was identified by comparing the mass spectra with the NIST library and also comparing the retention time with a commercially available liquid standard. MeSA was first calibrated using the calibration for (−)-alpha-pinene and then back calibrated using the relative response factor between (−)-alpha-pinene and MeSA. The workflow that was followed for sampling and sample analysis is given as a flow chart in Supplementary Fig. 7.

A detailed description of the sampling and analysis procedures for the 2017 and 2018 data is available in Zannoni et al., 2020[14].

The initial dates from January 8 to 13 2023 were chosen so that air samples could be collected from the canopy of the Amazon rainforest during the time of the Chemistry of the Atmosphere: Flight Experiment (CAFE) Brazil flight campaign which took place in the skies above Brazil from December 2022 – January 2023. Whilst we were in the Amazon rainforest during January 2023, there were reports that a strong El Niño event would likely hit the Amazon rainforest later in 2023. Therefore, the 2023–24 El Niño represented the ideal opportunity to try to understand how extreme abiotic stress conditions affect the alpha-pinene enantiomers in a pristine rainforest to further the work we had already undertaken in the Biosphere 2 tropical rainforest facility[15]. So, after January 8–13 2023 we tried to target as best we could with the available predictions and logistical constraints, the peak of the El Niño event (October 1–14 2023), the end of the El Niño event (April 16–May 4, 2024), and after the El Niño event (October 9–23 2024). We saw this as necessary so that we could capture an El Niño influenced wet and dry season, and a wet and dry season that were not influenced by an El Niño, while also capturing enough time periods to characterize the El Niño cycle from start to end.

Isoprene measurements at the tall tower

The isoprene measurements were conducted with a Proton Transfer Reaction Time of Flight Mass Spectrometer (PTR-Tof-MS; Ionicon Analytik, Innsbruck, Austria)[55]. The instrument was setup in an air-conditioned container at the base of the ATTO tower. Insulated and heated Teflon inlet lines (3/8″OD) were leading from the container to 80 m, 150 m and 325 m height on the ATTO tower. Each height is measured for 5 min. Each height is therefore sampled every 15 min for 5 min. Raw time resolution was 20 s but was subsequent averaged to one value for the respective 5-min period of one height. The average value was calculated by neglecting the first minute and last half minute of the 5 min period. This was done in order to eliminate any influence of the previous or upcoming height level measurement. The PTR-TOF-MS was operated with hydronium ions (H_3O^+) at a pressure of 2.2 mbar and an E/N of 120–130 Td. Mixing ratios of isoprene were obtained via calibrations with a gravimetrically prepared VOC calibration mixture (Apel-Riemer Environmental Inc., Colorado, USA) with an uncertainty of ≤20%. Precision of the measurement was ≤5% and the limit of detection ≤15ppt. Only the data from 80 m was used for this study. For comparison with the cartridge samples, the time periods were extracted and used that were closest to the cartridge sampling time periods. These time periods were January 1–31 2023, September 1–30 2023 and March 1–26 2024.

Drone measurements

Ambient air samples were collected using a homemade VOC-Sampler developed by the Max Planck Institute for Biogeochemistry, based on McKinney et al., and attached to an Unmanned Aerial Vehicle (UAV; Matrice 300 RTK, DJI)[56]. Air samples were taken with sorbent tubes packed with Tenax TA and Carbograph 5TD (Markes International, Inc.) for five min, with a flow rate of 150 sccm. Samples were collected in three forest types of the ATTO site and at three heights above the ground: for the upland forest at 35, 50, and 100 m; for the white-sand forest at 18, 50, and 100 m; and for the ancient river terrace forest at 30, 50, and 100 m[22]. The first height corresponds to the mean canopy height of each forest type. The UAV hovered for five min at each specified height while the VOC-sampler collected air samples, ensuring that sampling was only active during the hovering period. Blanks were also collected at each forest type to account for potential artifacts, such as the passive diffusion of monoterpenes into the sorbent tubes. For the blank samples, an uncapped sorbent tube was installed in one of the four sampling channels on the UAV-VOC-Sampler without sampling any air. Air sampling took place from October 8 to 17, 2024, with one flight conducted each day for each forest type between 12:00 and 13:30 local time (UTC-4). After collection, all tubes were capped with Swagelok fittings and PTFE ferrules and stored in an air-conditioned lab container.

Ozone and carbon dioxide measurements

CO_2 and O_3 concentrations were continuously monitored using a multi-height profile system located on the 80 m walk-up tower. The system comprised eight sampling heights, ranging from 0.05 m to 79 m, each equipped with a 3/8″ PTFE Teflon™ tube (Wolff Technik, Germany) and a 5 µm Teflon™ filter at the inlet. All tubes channelled air samples to a temperature-controlled container at the base of the tower, where the CO_2 and O_3 analysers were housed. A custom-built valve system governed sequential sampling from each inlet, consisting of a 3-way Teflon™ valve for each inlet, a Teflon™ membrane pump (KNF Neuberger, Germany), and a bypass pump (KNF Neuberger, Germany). Positioned outside the container, the Teflon™ pump drew air sequentially from each inlet, with valve operation coordinated by a CR3000X data logger (Campbell Scientific, USA). The data logger also managed the analysers and recorded measurement data. To mitigate water vapour interference in O_3 measurements and ensure dry air mixing ratios for O_3 and CO_2, a Nafion™ tube dryer system was installed. Additional 5 µm filters were placed before each analyser to prevent detector contamination and drift, with all filters replaced biweekly as part of routine maintenance. The system completed a full measurement cycle across all heights every 16 min for the first three cycles and 12 min for the final cycle, resulting in four complete cycles per hour. Sampling at each height lasted 2 min for the first three cycles and 1.5 min for the fourth cycle. The first minute of each measurement was discarded to eliminate artefacts from valve switching, while the bypass pump continually flushed the inactive sampling line in preparation for the next measurement.

For this study, data from the 24 m inlet of the long-term reactive profile measurement system were used, as this height was closest to the VOC sampling inlet. Additionally, CO_2 data from 0.5 m were included for the gradient calculations.

Ozone measurements were performed using a TEI 49iC ozone monitor (Thermo Fisher Scientific, USA), which operates via ultraviolet (UV) absorption. The instrument has a detection limit of 1.0 ppb and a linearity of ±2 ppb. A 2B Model 306 ozone calibration source (2B Technologies, USA) was used for periodic calibrations. The accuracy of the ozone measurements, as specified by the manufacturer, is the greater of 2 ppbv or 2% of the ozone concentration. Two-sigma precision is 0.5 ppbv in 1 min.

CO_2 concentrations were measured with a LI-COR LI-7000 (LI-COR Environmental, USA), a differential, non-dispersive infrared (NDIR) gas analyser designed for high-precision quantification of CO_2 in air samples. The analyser was calibrated regularly, with relevant calibrations conducted on 7 October 2022 and 14 February 2023. Calibration utilised certified standard gases (Saphir gas mixture, Air Liquide, Germany) containing 340.9, 450.5, and 580.5 mol-ppm of CO_2, all with an uncertainty of ±1%. And for the zero-air calibration, synthetic air was used, with CO_2 <0.5 ppm. We determine the measurement accuracy to be ±1%, with a two-sigma precision in 1 minute of 8 ppmv.

Stomatal conductance measurements

Measurements were performed on 12 trees from 12 species of angiosperm (one tree/species) (Supplementary Table 1), 6 brevideciduous and 6 evergreen trees, during the late dry season between 14th September and 21st September 2023. These trees were located around the 80 m walk-up tower and details on leaf phenological types can be found elsewhere[52]. Given the logistical challenges of studying tall tropical trees, often exceeding 20 meters in height, all measurements were performed on leaf samples collected from cut branches immediately placed in water. This method provided a practical solution for conducting gas exchange measurements without compromising leaf viability[22,52,57–60]. With the help of a tree climber, branches with at least 2 cm diameter were collected from sun-exposed areas of the canopy to avoid shade-adapted leaves. Senescent, young, or visibly damaged leaves were excluded, ensuring that only physiologically active leaves were analysed. After collection, branches were immediately re-cut underwater to prevent embolism, stored in water bottles for transport, and re-cut once more under water at the field camp to restore xylem flow before measurements. Leaves displaying reduced physiological activity were excluded from analysis, minimizing potential artifacts due to branch excision. For each tree, one visibly mature and healthy leaf of the branch was selected for measurement.

The leaf gas exchange characteristics were measured using a LI-6800 portable gas exchange system (LiCor Inc., USA) with a hydrocarbon filter (Restek Pure Chromatography, Restek Corporations, USA) installed at the inlet of the gas analyser to remove contaminants from incoming ambient air. All tubing in contact with the sampling air was PTFE and did not exchange contaminants.

Each leaf was separately enclosed (for compound leaves we considered a leaflet as the equivalent of a simple leaf lamina) in the leaf chamber with the following environmental conditions: photosynthetic photon flux density (PPFD) of 1000 mmol m^{-2} s^{-1}, leaf temperature of 30 °C, flow rate of air going into the leaf chamber of 500 mmol s^{-1}, CO_2 and H_2O concentrations of 420 mmol mol^{-1} and 21 mmol mol^{-1}, and relative humidity of ~60%; beginning measurements after acclimating the leaf to these conditions for at least 20 min, until net assimilation (A_n), stomatal conductance (g_s) and internal CO_2 concentration (C_i) reached a stable, positive plateau. Gas exchange characteristics were measured at different temperature conditions: 30.0, 35.0, 37.5, 40.0, 42.5, and 45.0 °C; while fixing light (1000 µmol m^{-2} s^{-1}), CO_2 (420 ppm), and relative humidity (~60%). System values were logged every 30 s for 5 min at each step of the temperature curve. In total 2198 measurements were obtained, with 1000 points from the local morning and 1198 points from the local afternoon. Measurements were performed at varied temperatures across time-of-day. All data was then sorted by time-of-day and a moving median was performed on the data with a window size of 200. The resulting data was then averaged to every 30 min, and the 25th and 75th percentiles were calculated for each 30 min of data. This was done to show the combined stomatal conductance trend across time-of-day for all of the leaves that were measured during this time period.

Reporting summary

Further information on research design is available in the Nature Portfolio Reporting Summary linked to this article.

Data availability

The data used to support the findings in this study are publicly available on the ATTO data portal and can be accessed with the following DOIs: Alpha-pinene and MeSA data January 2023: https://doi.org/10.17871/ATTO.511.16.2161, Alpha-pinene and MeSA data October 2023: https://doi.org/10.17871/ATTO.512.10.2162, Alpha-pinene and MeSA data April–May 2024: https://doi.org/10.17871/ATTO.513.10.2163, Alpha-pinene and MeSA data October 2024: https://doi.org/10.17871/ATTO.514.9.2164, Isoprene data: https://doi.org/10.17871/ATTO.557.8.2233. Temperature, Relative humidity and Soil moisture data from 2022-2024: https://doi.org/10.17871/ATTO.556.7.2213. Temperature, relative humidity, photosynthetically active radiation, soil moisture, and ozone data during the VOC sampling periods: https://doi.org/10.17871/ATTO.516.8.2158, CO_2 data: https://doi.org/10.17871/ATTO.518.10.2167, Stomatal conductance data: https://doi.org/10.17871/ATTO.520.6.2143, Alpha-pinene mixing ratios collected with drone around ATTO Site, covering three vegetation types (upland, white-sand and ancient river terrace forests) at three different heights in October 2024: https://doi.org/10.17871/ATTO.522.8.2168. Dry and wet seasons datasets of (−)-α-pinene and (+)-α pinene from 2017 and 2018 campaigns are accessible at: https://doi.org/10.17871/atto.150.5.558, https://doi.org/10.17871/atto.151.3.559, https://doi.org/10.17871/atto.139.4.561, https://doi.org/10.17871/atto.143.5.560.

Received: 27 May 2025; Accepted: 13 August 2025;
Published online: 26 August 2025

References

1. Morley, R. J. *Origin and Evolution of Tropical Rain Forests* (John Wiley & Sons, 2000).
2. Nobre, C. et al. *Amazon Assessment Report 2021, Vol.* 55161 (UN Sustainable Development Solutions Network (SDSN), 2021).
3. Gatti, L. V. et al. Amazonia as a carbon source linked to deforestation and climate change. *Nature* **595**, 388–393 (2021).
4. Malhi, Y. & Grace, J. Tropical forests and atmospheric carbon dioxide. *Trends Ecol. Evol.* **15**, 332–337 (2000).
5. IPCC Climate Change. *The Physical Science Basis: Working Group I Contribution to the Sixth Assessment Report of the Intergovernmental Panel on Climate Change* (Cambridge University Press, 2023).
6. Duffy, P. B. et al. Projections of future meteorological drought and wet periods in the Amazon. *Proc. Natl. Acad. Sci.* **112**, 13172–13177 (2015).
7. Cai, W. et al. ENSO and greenhouse warming. *Nat. Clim. Change* **5**, 849–859 (2015).
8. Guenther, A. et al. The Model of emissions of gases and aerosols from nature version 2.1 (MEGAN2. 1): an extended and updated framework for modeling biogenic emissions. *Geosci. Model Dev.* **5**, 1471–1492 (2012).
9. Peñuelas, J. & Staudt, M. BVOCs and global change. *Trends Plant Sci.* **15**, 133–144 (2010).
10. Cruz de Carvalho, M. H. Drought stress and reactive oxygen species: Production, scavenging and signaling. *Plant Signal. Behav.* **3**, 156–165 (2008).
11. Huang, H. et al. Mechanisms of ROS regulation of plant development and stress responses. *Front. Plant Sci.* **10**, 800 (2019).
12. Gill, S. S. & Tuteja, N. Reactive oxygen species and antioxidant machinery in abiotic stress tolerance in crop plants. *Plant Physiol. Biochem.* **48**, 909–930 (2010).
13. Niinemets, Ü, Loreto, F. & Reichstein, M. Physiological and physicochemical controls on foliar volatile organic compound emissions. *Trends Plant Sci.* **9**, 180–186 (2004).
14. Zannoni, N. et al. Surprising chiral composition changes over the Amazon rainforest with height, time and season. *Commun. Earth Environ.* **1**, 4 (2020).
15. Byron, J. et al. Chiral monoterpenes reveal forest emission mechanisms and drought responses. *Nature* **609**, 307–312 (2022).

16. Yáñez-Serrano, A. M. et al. Monoterpene chemical speciation in a tropical rainforest:variation with season, height, and time of dayat the Amazon Tall Tower Observatory (ATTO). *Atmos. Chem. Phys.* **18**, 3403–3418 (2018).
17. Williams, J. et al. Mirror image hydrocarbons from Tropical and Boreal forests. *Atmos. Chem. Phys.* **7**, 973–980 (2007).
18. Espinoza, J.-C. et al. The new record of drought and warmth in the Amazon in 2023 related to regional and global climatic features. *Sci. Rep.* **14**, 8107 (2024).
19. Jiménez-Muñoz, J. C. et al. Record-breaking warming and extreme drought in the Amazon rainforest during the course of El Niño 2015–2016. *Sci. Rep.* **6**, 33130 (2016).
20. Jardine, K. J. et al. Monoterpene 'thermometer' of tropical forest-atmosphere response to climate warming. *Plant Cell Environ.* **40**, 441–452 (2017).
21. Werner, C. et al. Ecosystem fluxes during drought and recovery in an experimental forest. *Science* **374**, 1514–1518 (2021).
22. Gomes Alves, E. et al. Seasonal shifts in isoprenoid emission composition from three hyperdominant tree species in central Amazonia. *Plant Biol.* **24**, 721–733 (2022).
23. Bao, X. et al. A meta-analysis on plant volatile organic compound emissions of different plant species and responses to environmental stress. *Environ. Pollut.* **318**, 120886 (2023).
24. Karl, T. et al. Chemical sensing of plant stress at the ecosystem scale. *Biogeosciences* **5**, 1287–1294 (2008).
25. Holopainen, J. K. & Gershenzon, J. Multiple stress factors and the emission of plant VOCs. *Trends Plant Sci.* **15**, 176–84 (2010).
26. Ren, Y. et al. The fate of methyl salicylate in the environment and its role as signal in multitrophic interactions. *Sci. Total Environ.* **749**, 141406 (2020).
27. Pfannerstill, E. Y. et al. Total OH reactivity changes over the amazon rainforest during an El Niño event. *Front. For. Glob. Change* **1**, 12 (2018).
28. Engelberth, J. & Engelberth, M. Variability in the Capacity to Produce Damage-Induced Aldehyde Green Leaf Volatiles among Different Plant Species Provides Novel Insights into Biosynthetic Diversity. *Plants* **9**, 213 (2020).
29. Yáñez-Serrano, A. M. et al. Heat stress increases the use of cytosolic pyruvate for isoprene biosynthesis. *J. Exp. Bot.* **70**, 5827–5838 (2019).
30. Andreae, M. O. et al. The Amazon Tall Tower Observatory (ATTO): overview of pilot measurements on ecosystem ecology, meteorology, trace gases, and aerosols. *Atmos. Chem. Phys.* **15**, 10723–10776 (2015).
31. Rummel, U. et al. Seasonal variation of ozone deposition to a tropical rain forest in southwest Amazonia. *Atmos. Chem. Phys.* **7**, 5415–5435 (2007).
32. Ghirardo, A. et al. Determination of de novo and pool emissions of terpenes from four common boreal/alpine trees by 13CO2 labelling and PTR-MS analysis. *Plant Cell Environ.* **33**, 781–792 (2010).
33. Noe, S. M. et al. Emissions of monoterpenes linalool and ocimene respond differently to environmental changes due to differences in physico-chemical characteristics. *Atmos. Environ.* **40**, 4649–4662 (2006).
34. Staudt, M. et al. New insights into the parametrization of temperature and light responses of mono - and sesquiterpene emissions from Aleppo pine and rosemary. *Atmos. Environ.* **152**, 212–221 (2017).
35. Sander, R. Compilation of Henry's law constants (Version 4.0) for water as solvent. *Atmos. Chem. Phys.* **15**, 4399–4981 (2015).
36. Selmar, D. & Kleinwächter, M. Stress Enhances the Synthesis of Secondary Plant Products: The Impact of Stress-Related Over-Reduction on the Accumulation of Natural Products. *Plant Cell Physiol.* **54**, 817–826 (2013).
37. de Souza, V. F. et al. Photosynthetic Temperature Tolerance Threshold Determines How Isoprene Emission is Affected by Elevated CO2 Concentration at High Temperatures. *Plant-Environ. Interact.* **6**, e70053 (2025).
38. Agurla, S., Sunitha, V. & Raghavendra, A. S. Methyl salicylate is the most effective natural salicylic acid ester to close stomata while raising reactive oxygen species and nitric oxide in Arabidopsis guard cells. *Plant Physiol. Biochem.* **157**, 276–283 (2020).
39. Sharkey, T. D. & Yeh, S. S. Isoprene emission from plants. *Annu. Rev. Plant Physiol. Plant Mol. Biol.* **52**, 407–436 (2001).
40. Kuhn, U. et al. Isoprene and monoterpene fluxes from Central Amazonian rainforest inferred from tower-based and airborne measurements, and implications on the atmospheric chemistry and the local carbon budget. *Atmos. Chem. Phys.* **7**, 2855–2879 (2007).
41. Gonçalves, N. B. et al. Both near-surface and satellite remote sensing confirm drought legacy effect on tropical forest leaf phenology after 2015/2016 ENSO drought. *Remote Sens. Environ.* **237**, 111489 (2020).
42. Rivera, G. et al. Increasing day-length induces spring flushing of tropical dry forest trees in the absence of rain. *Trees* **16**, 445–456 (2002).
43. Lian, X., Morfopoulos, C. & Gentine, P. Water deficit and storm disturbances co-regulate Amazon rainforest seasonality. *Sci. Adv.* **10**, eadk5861 (2024).
44. Borchert, R., Rivera, G. & Hagnauer, W. Modification of vegetative phenology in a tropical semi-deciduous forest by abnormal drought and rain. *Biotropica* **34**, 27–39 (2002).
45. Meza-Elizalde, M. C. & Armenteras-Pascual, D. Edge influence on the microclimate and vegetation of fragments of a north Amazonian forest. *For. Ecol. Manag.* **498**, 119546 (2021).
46. Hofmeister, J. et al. Microclimate edge effect in small fragments of temperate forests in the context of climate change. *For. Ecol. Manag.* **448**, 48–56 (2019).
47. Schedlbauer, J. L. & Miller, J. Edge effects increase soil respiration without altering soil carbon stocks in temperate broadleaf forests. *Ecosphere* **13**, e4092 (2022).
48. Bougas, L. et al. Absolute optical chiral analysis using cavity-enhanced polarimetry. *Sci. Adv.* **8**, eabm3749 (2022).
49. Seco, R. et al. Ecosystem-scale volatile organic compound fluxes during an extreme drought in a broadleaf temperate forest of the Missouri Ozarks (central USA). *Glob. Change Biol.* **21**, 3657–3674 (2015).
50. ter Steege, H. et al. Hyperdominance in the Amazonian tree flora. *Science* **342**, 1243092 (2013).
51. Bourtsoukidis, E. et al. High temperature sensitivity of monoterpene emissions from global vegetation. *Commun. Earth Environ.* **5**, 23 (2024).
52. Robin, M. et al. Interactions between leaf phenological type and functional traits drive variation in isoprene emissions in central Amazon forest trees. *Front. Plant Sci.* **15**, 1522606 (2024).
53. Kesselmeier, J. et al. Concentrations and species composition of atmospheric volatile organic compounds (VOCs) as observed during the wet and dry season in Rondônia (Amazonia). *J. Geophys. Res. Atmos.* **107**, LBA 20-1–LBA 20-13 (2002).
54. Ernle, L., Ringsdorf, M. A. & Williams, J. Influence of ozone and humidity on PTR-MS and GC-MS VOC measurements with and without a $Na_2S_2O_3$ ozone scrubber. *Atmos. Meas. Tech.* **16**, 1179–1194 (2023).
55. Jordan, A. et al. A high resolution and high sensitivity proton-transfer-reaction time-of-flight mass spectrometer (PTR-TOF-MS). *Int. J. Mass Spectrom.* **286**, 122–128 (2009).
56. McKinney, K. A. et al. A sampler for atmospheric volatile organic compounds by copter unmanned aerial vehicles. *Atmos. Meas. Tech.* **12**, 3123–3135 (2019).
57. Jardine, K. J. et al. Leaf isoprene and monoterpene emission distribution across hyperdominant tree genera in the Amazon basin. *Phytochemistry* **175**, 112366 (2020).

58. Taylor, T. C. et al. A new field instrument for leaf volatiles reveals an unexpected vertical profile of isoprenoid emission capacities in a tropical forest. *Front. For. Glob. Change* **4**, 668228 (2021).
59. Llusia, J. et al. A screening study of leaf terpene emissions of 43 rainforest species in Danum Valley conservation area (Borneo) and their relationships with chemical and morphological leaf traits. *Plant Biosyst. Int. J. Deal. Asp. Plant Biol.* **148**, 307–317 (2014).
60. Albert, L. P. et al. Age-dependent leaf physiology and consequences for crown-scale carbon uptake during the dry season in an Amazon evergreen forest. *N. Phytol.* **219**, 870–884 (2018).
61. NOAA (National Oceanic and Atmospheric Administration). NOAA (National Oceanic and Atmospheric Administration). (accessed 06 Jan 2025). https://origin.cpc.ncep.noaa.gov/products/analysis_monitoring/ensostuff/ONI_v5.php.

Acknowledgements

This research has been funded by the Bundesministerium für Bildung und Forschung (01LB1001A, 01LK1602B, and 01LK2101B), the Brazilian Ministério da Ciência, Tecnologia e Inovação (01.11.01248.00), and the Max Planck Society. Operation of the ATTO site was supported by the Instituto Nacional de Pesquisas da Amazônia (INPA), the Conselho Nacional de Desenvolvimento Científico e Tecnológico (CNPq), the Amazon State University (UEA), the Large-Scale Biosphere-Atmosphere Experiment (LBA), Fundação de Amparo à Pesquisa do Estado de Amazonas (FAPEAM), the Reserva de Desenvolvimento Sustentável do Uatumã (SDS/CEUC/RDS-Uatumã), and the Max Planck Society. We would like to give thanks to the ATTO team members: Reiner Ditz, Sipko Bulthuis, Christopher Pöhlker, Sebastian Brill, Jana Englert, Dennis Geis, and Björn Nillius and all further colleagues involved in the technical, logistical, and scientific support. Stefan Sala and Andreas Engel are acknowledged for developing the software IAU_Chrom used to integrate the chromatograms peak areas.

Author contributions

J.B., G.P., and J.W. conceived and designed the study. J.B., G.P., J.S., and S.C.H. collected and processed the VOC samples from the walk-up tower. J.B. and N.Z. collected and processed the VOC samples from the tall tower campaign in 2017. N.Z. collected and analysed the samples from the tower campaign in 2018. E.G.A. collected the drone samples and J.B. processed and analysed them. M.R. provided the stomatal conductance data. A.E. provided the isoprene data. C.Q.D.J. and C.A.Q. provided the meteorological data. C.A.M., A.T., and H.H. provided the CO_2 and ozone data. J.B. curated the VOC data, and conducted the formal analysis and visualisation of the data. J.B., G.P., B.E.K., E.B., E.G.A., and J.W. discussed and interpreted the data. JL and JW acquired the funding. J.B. wrote the original draft manuscript. All authors contributed to writing and editing the final manuscript.

Funding

Open Access funding enabled and organized by Projekt DEAL.

Competing interests

Nora Zannoni is an Editorial Board Member for Communications Earth & Environment, but was not involved in the editorial review of, nor the decision to publish this article. All other authors declare no competing interests.

Additional information

Supplementary information The online version contains supplementary material available at https://doi.org/10.1038/s43247-025-02709-z.

Correspondence and requests for materials should be addressed to Joseph Byron or Jonathan Williams.

Peer review information *Communications Earth and Environment* thanks the anonymous reviewers for their contribution to the peer review of this work. Primary Handling Editor: Alice Drinkwater. A peer review file is available.